Journal of Materials Chemistry A

Judicious Selection of Bifunctional Molecules to Chemically Modify Graphene for Improving Nanomechanical and Thermal Properties of Polymer Composites

Journal:	*Journal of Materials Chemistry A*
Manuscript ID:	TA-ART-09-2014-004543.R1
Article Type:	Paper
Date Submitted by the Author:	23-Sep-2014

Complete List of Authors:	Yang, Yingkui; Hubei University, Faculty of Materials Science and Engineering He, Cheng-En; Hubei University, Faculty of Materials Science and Engineering Tang, Wei; Hubei University, Faculty of Materials Science and Engineering Tsui, Chi-Pong; The Hong Kong Polytechnic University, Shi, Dean; Hubei University, sun, Zhengguang; Faculty of Materials Science &Engineering, Hubei University Jiang, Tao; Hubei University, Xie, Xiaolin; HUST, School of Chemistry and Chemical Engineering

Judicious Selection of Bifunctional Molecules to Chemically Modify Graphene for Improving Nanomechanical and Thermal Properties of Polymer Composites

Yingkui Yang,[*ab] Cheng-En He,[ac] Wei Tang,[a] Chi Pong Tsui,[*b] Dean Shi,[a] Zhengguang Sun,[a] Tao Jiang,[a] and Xiaolin Xie[c]

[a] *MOE Laboratory for Green Preparation and Application of Functional Materials, Hubei Collaborative Innovation Center for Advanced Organic Chemical Materials, and Faculty of Materials Science and Engineering, Hubei University, Wuhan 430062, China*

E-mail: yingkuiyang@gmail.com

[b] *Department of Industrial and Systems Engineering, The Hong Kong Polytechnic University, Hung Hom, Kowloon, Hong Kong, China*

E-mail: gary.c.p.tsui@polyu.edu.hk

[c] *State Key Laboratory of Materials Processing and Die & Mould Technology, and School of Chemistry and Chemical Engineering, Huazhong University of Science and Technology, Wuhan 430074, China*

Abstract

Covalently-functionalized graphene (FG) was successfully obtained by grafting *m*-isopropenyl-α, α'-dimethyl benzyl isocyanate (*m*-TMI) to graphene oxide (GO) followed by chemical and solvothermal reduction of GO. FG sheets were hydrophobic and stable in polar solvents such as *N*, *N*-dimethylformamide. Reactive vinyl-benzyl groups of *m*-TMI attached to FG were copolymerized with methyl methacrylate to produce graphene/poly(methyl methacrylate) (PMMA) composites. FG sheets were well dispersed in PMMA and form strong interface bonding with the matrix, thus contributing to large increases in elastic modulus (+72.9%) and indentation hardness (+51.2%) at 1% loading in weight. Incorporation of FG into PMMA changed its elastic-plastic behavior and hence, a decrease of plasticity index and an increase of recovery resistance were observed for the resulted composites due to the increased portion related to the elastic work. The onset decomposition temperature and glass transition temperature of neat PMMA also increase by 100°C and 12.7°C, respectively, by addition of 1 wt% FG. Herein, *in-situ* copolymerization of monomers and well-suspended FG promotes the exfoliation of graphene associated with a strong chemical bonding with the polymer matrix. This promises a facile method for fabricating high-performance polymeric composites.

1. Introduction

Graphene has been known as an atomically thick and two-dimensional sheet composed of sp^2-hybridized carbon atoms arranging in a honeycomb crystal lattice.[1] It is structurally similar to carbon nanotubes (CNTs) and dimensionally analogous to layered clays and hence, showing the combined properties of CNTs (electrical, thermal and mechanical reinforcements) and clays (stiffness, gas impermeability and low cost). These extraordinary properties plus extremely high specific-surface-area have made graphene more attractive for improving the mechanical, electrical, thermal, and gas barrier properties of polymers.[2] Till now, graphene has been successfully produced by solid-/liquid-phase exfoliation of graphite, epitaxial growth, chemical vapor deposition, and reduction of graphene oxide (GO).[3] However, graphene/polymer composites have been predominately fabricated using reduced GO (RGO) by melt processing, solution mixing and *in-situ* polymerization techniques over the past decade.[4]

For effectively improving the host polymer, however, homogeneous dispersion of graphene in the matrix is a prerequisite for the uniform and fast stress distribution throughout the composite.[5, 6] Although GO sheets are readily dispersed in water or organic solvents due to the presence of oxygenated functional groups around its basal plane and edges, bulk graphene sheets from RGO often agglomerate into large clusters irreversibly and even tend to restack as a graphite-like structure because of attractive van der Waals interactions between the sheets.[2] Besides, the strong graphene-matrix interface is highly desirable to provide effective load transfer and great reinforcement effects. The critical challenge for graphene/polymer composites thus lies in uniformly exfoliating graphene sheets into the matrix to produce strong interfacial bonding between two components.[5] Some researchers have attempted to directly mix GO with polymers in solution followed by chemical and thermal reduction of GO to obtain graphene/polymer composites, but the

in-situ reduction techniques could cause polymer degradation arising from chemical reductants and high processing temperature.[7]

Currently improved strategies are to functionalize graphene with organic molecules and polymers by non-covalent and covalent methodologies.[2] Non-covalent functionalization with the modified reagents can weaken van der Vaals forces between graphene sheets and enhance their dispersibility in solvents and polymers. However, non-covalent interactions including hydrophobic, electrostatic interactions and π-π stacking result in the weak graphene-matrix interface adhesion and low efficiency of load transfer between the two phases. Meanwhile, some residual additives such as surfactants would decrease the improvement effect on the composites. In contrast, covalent functionalization involves a strong chemical attachment of functional molecules to the π-conjugated skeleton of graphene. The grafted chains could be entangled with the matrix polymer chains acting as many bridges between the graphene and matrix, and become an integral part of the matrix. Covalently-functionalized graphene makes the resultant composites more stable and hence, is superior in the improvement of the material properties.[8]

Over the past years, covalent grafting of polymer chains to graphene sheets has been successfully performed by either grafting-from or grafting-to strategies.[2] The grafting-to approach involves polymer synthesis prior to grafting, but shows a low graft density due to the chains' steric hindrance. The grafting-from technique derives from the activated graphene or the graphene-supported macroinitiators which initiate surface polymerization of monomers to yield the tethered polymer chains, thus affording a relatively higher graft density. Marques *et al.*[9] pretreated GO with acyl chloride followed by reaction with ethylene glycol and 2-bromo-2-methylpropionyl bromide in turn. The resulting bromide-activated GO could trigger atom transfer radical polymerization (ATRP) of MMA to yield soluble PMMA-grafted GO sheets. Incorporation of 1 wt%

functionalized graphene into the PMMA matrix contributed to increases by 21.8% for Young's modulus and 42% for tensile strength, respectively. Lu *et al.*[10] synthesized the bromide bonded-graphene by aryl diazonium addition and acylation with 2-bromopropionyl bromide. Subsequent ATRP reaction allowed PS chains to grow from the graphene surface. PS-grafted graphene sheets were then mixed with PS to obtain graphene/PS composites with enhanced thermal conductivities and glass transition temperatures (T_g). However, using living polymerization techniques such as ATRP to obtain polymer-grafted graphene seem relatively complicated in practice and are also inappropriate for scaled-up production.

Recently, Song *et al.*[11] synthesized vinyl-functionalized GO by a silane-coupling reaction of γ-methacryloxypropyl trimethoxysilane (MPS) with an aqueous suspension of GO. Afterwards, they carried out a miniemulsion copolymerization in the presence of MPS-modified GO followed by *in-situ* reduction to obtain poly(styrene-*co*-methyl methacrylate) (PS-*co*-PMMA) grafted RGO. The copolymer grafted RGO sheets were finally added to the immiscible PS/PMMA blend to prepare conductive polymer composites having a very low percolation threshold (0.02 vol%). Jiang *et al.*[12] synthesized vinyl-modified graphene by an esterification of acyl-activated GO with 2-hydroxyethyl acrylate followed by an emulsion copolymerization with MMA. The resultant PMMA-grafted graphene sheets were then melt-blended with PMMA to produce graphene/PMMA composites with increases by 31% and 27% for tensile strength and storage modulus, respectively, upon 1 wt% loading. Vinyl-functionalized graphene sheets are widely applicable for the mass production of polymer composites since many polymers have been commercially produced by free radical polymerization. However, several disadvantages are associated with the above work: i) dangerous acylation of GO using acyl chloride; ii) low density of functional groups because only COOH groups of GO were used for acylation and one functional molecule of MPS reacted with several OH

and COOH groups of GO; iii) side reactions due to self-polymerization (*e.g.*, MPS, acrylates) and self-condensation (*e.g.*, MPS) during functionalization of graphene; iv) multiple steps including acylation-esterification or hydrolysis-condensation reactions. It is of significantly importance to develop an efficient method for the functionalization of graphene for polymer composites.

In this study, we report a new, facile method to produce covalently-functionalized graphene (FG) using a bifunctional molecule of *m*-isopropenyl-α, α'-dimethyl benzylisocyanate (*m*-TMI) after chemical and solvothermal reduction of GO. Several benefits are associated with our work: i) *m*-TMI does not homopolymerize by radical initiators or heating due to its steric hindrance of *α*-methyl group;[13, 14] ii) the isocyanate (NCO) group of *m*-TMI is less sensitive to water because of the adjacent isopropyl group;[13] iii) GO covers many hydroxyl and carboxyl groups which are available for reacting with NCO of *m*-TMI,[15, 16] and iv) vinyl-benzyl groups of *m*-TMI easily copolymerize with vinyl monomers such as acrylates and styrene. The first three characteristics result in a high functionalization degree due to the lack of side reactions and high reactivity. The *m*-TMI modified graphene sheets show a highly improved capacity to form stable suspensions in polar solvents. These make *m*-TMI an ideal chemical scaffold for surface modification through free-radical copolymerization with vinyl monomers, facilitating the preparation of graphene polymer composites. Furthermore, the nanoindentation technique was performed using a Berkovich indenter to examine the mechanical properties of composites in nano-scales, such as elastic modulus, hardness, and elastic-plastic behaviors.

2. Experimental

2.1. Materials

Graphite powder (<20 μm), *m*-isopropenyl-α, α'-dimethyl benzylisocyanate (*m*-TMI; 95%),

dimethyl hydrazine (98%) and dibutyltin dilaurate (DBTDL; 95%) were purchased from Sigma-Aldrich and used as-received. Graphene oxide (GO) was prepared from graphite by a modified Hummers method.[17, 18] Methyl methacrylate (MMA; 99%, Aldrich) was purified by filtering over the alumina powder to remove the inhibitors before use. 2, 2-Azobis(isobutyronitrile) (AIBN; 98%, Aldrich) was re-crystallized from ice methanol. *N*, *N*-Dimethylformamide (DMF) was kept in 4-Å molecular sieves and then distilled by reduced-pressure before use.

2.2. Functionalization of graphene with m-TMI

Dried GO (400 mg) was ultrasonically dispersed in anhydrous DMF (70 mL) to obtain a stable suspension. A solution of *m*-TMI (2 mL, 10.1 mmol) and DBTDL (0.3 mL) in anhydrous DMF (10 mL) was added to the GO suspension, and the mixture was stirred for 24 h at 50°C under nitrogen atmosphere. To the above suspension, dimethylhydrazine (1 mL) was directly added and then allowed to stand for 16 h at 80°C followed by refluxing for 2 h at 150°C with constant stirring. The obtained black dispersion was subjected to several cycles of filtration and washing with DMF and acetone to remove residual *m*-TMI and organic impurities. Finally, *m*-TMI-functionalized graphene (*abbreviated as* FG) sheets were obtained by drying in vacuum.

2.3. Preparation of graphene/PMMA composites

FG sheets were readily dispersed and exfoliated in DMF (2 mg/mL) by sonication in a bath at room temperature. An appropriate amount of MMA monomer with 0.5 wt% AIBN was added to the FG dispersion by magnetic stirring and the mixture was deoxygenated by vacuum/dry nitrogen for several cycles in a water-ice bath. The flask charged with the above reactants was placed in a preheated oil bath at 70°C to perform free radical polymerization under nitrogen atmosphere and constant stirring. After 12 h reaction, the black solution was poured into a large volume of

vigorously-stirred ice methanol to produce a grey-black precipitate. Finally, the coagulated graphene/PMMA composite powders were achieved by filtration and drying overnight at 70°C. For the comparison purpose, neat PMMA was also prepared by the same experimental condition in the absence of FG.

2.4. Characterization

Transmission electron microscopy (TEM) analysis was performed on a Tecnai G220 electron microscope at 200 kV. Atomic force microscopy (AFM) images were recorded using Digital Instrument Nanoscope IIIA Atomic Force Microscope operating in a tapping mode. The morphologies of the fresh-fractured surface of the composites were determined by scanning electron microscopy (SEM, Quanta200, FEI) using a charge contrast imaging mode. X-ray diffraction (XRD) experiments were conducted in a D/MAX-IIIC X-ray diffractometer with Cu Kα radiation. X-ray photoelectron spectroscopy (XPS) was performed on a Physical Electronics spectrometer (PHI 5082) using a monochromatic Al Kα X-ray source. Thermal gravimetric analysis (TGA) was conducted using a PE TGA-7 calorimeter under argon flow (20 mL/min) at a heating rate of 10°C/min. Differential scanning calorimetry (DSC) was carried out on a PE DSC-7 calorimeter at 10°C/min in an argon atmosphere. Optical pictures were recorded with a digital camera (Sony DSC-TX10).

For the nanoindentation measurements on PMMA and its composites, the powder materials were compressed into thin films of ~2.5 mm thickness by a hot press at 190°C for 6-8 minutes. These films were then cut into small specimens with 10×10 mm^2 area. Nanoindentation tests were performed on a MTS Nano-Indenter XP instrument (USA) equipped with a diamond Berkovich indenter under ambient conditions. The tip contact area function was calibrated by a fused-quartz standard specimen before measurements. It should be noted that nanomechanical properties of polymer-based materials are sensitive to the penetration rate and depth,[19] these indentation

parameters such as loading and unloading rates and holding time at the peak load were assessed by available literature data.[20-22] The indenter was herein penetrated into the specimen at a low constant loading rate (0.05 nm/s) and strain rate (0.1/s) until a maximum penetration-depth (h_m) of 2000 nm was reached. The h_m value is less than 1/10 of specimen thickness to avoid the influence of substrate used.[23] The load holding at h_m was set for 10 s to minimize the time-dependent plastic effect, and the tip was then removed from the sample surface at the same rate during unloading. Ten indentations were conducted on different points for each specimen to calculate the average values of nanomechanical properties using the Oliver-Pharr method.[24]

3. Results and Discussion

3.1. Functionalized graphene for fabricating PMMA composites

Figure 1 shows the synthesis procedure of functionalized graphene. Chemical oxidation of graphite to graphite oxide was first performed by a modified Hummers method.[17, 18] Direct exfoliation of graphite oxide via ultra-sonication produces monolayer GO sheets which are readily dispersed in water and organic solvents such as DMF due to the hydrophilicity, ionizability and polarity of oxygen-containing groups.[25-27] However, bulk graphene sheets from reduced GO tend to restack as a graphite-like structure and show low dispersibility in solvents due to the disappearance of many functional groups after reduction.[28] Unlike most other work reported,[29-32] therefore, functionalization with *m*-TMI was carried out before reduction of GO in this work. Both hydroxyl and carboxyl groups of GO readily react with NCO group of *m*-TMI in DMF to form carbamate and amide bonds, respectively. Residual oxygen functional groups within *m*-TMI-derived GO can be effectively removed by chemical reduction with dimethylhydrazine [15] and solvothermal reduction in DMF at an elevated temperature,[33, 34] thus obtaining *m*-TMI-functionalized graphene (FG).

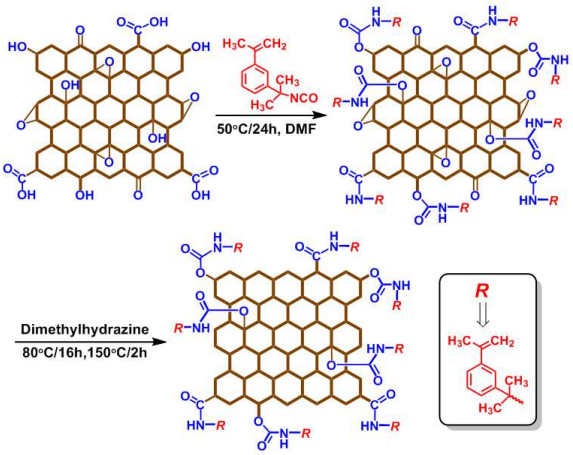

Figure 1. Schematic illustration for grafting of *m*-TMI onto GO and subsequent reduction of GO to produce *m*-TMI-functionalized graphene (FG).

GO sheets are well stable in water to form a luminous-yellow solution (Fig. 2d), and the average height measured on a mica substrate is ~0.86 nm corresponding to monolayer sheets (Fig. 2a). Coupling with *m*-TMI and reduction, however, reduce GO's hydrophilicity, and the resulted FG sheets are no longer dispersed into water but readily form stable black suspensions in polar solvents such as DMF (Fig. 2d). Completely exfoliated FG sheets possess an average height of ~1.34 nm as determined by AFM (Fig. 2b). An atomic pristine graphene sheet is known to have a theoretically predicted thickness of 0.34 nm, but GO and FG monolayer sheets are apparently thicker for comparison. The former is ascribed to the presence of large amounts of oxygen-containing groups on both planes, while the latter is assigned to the covalent attachment of *m*-TMI to graphene. Moreover, the increased sheet thickness of FG by 0.48 nm relative to that of GO comes from larger molecular size of *m*-TMI instead of oxide groups of GO. A typical TEM image illustrates the featureless basal plane and a monolayer edge of FG (Fig. 2c) in accordance with the AFM result. Besides, the selected area electron diffraction (SAED) shows a well-defined diffraction spots (inset in Fig. 2c), revealing the graphitic laminar nature of FG made by reduction of GO.[35, 36]

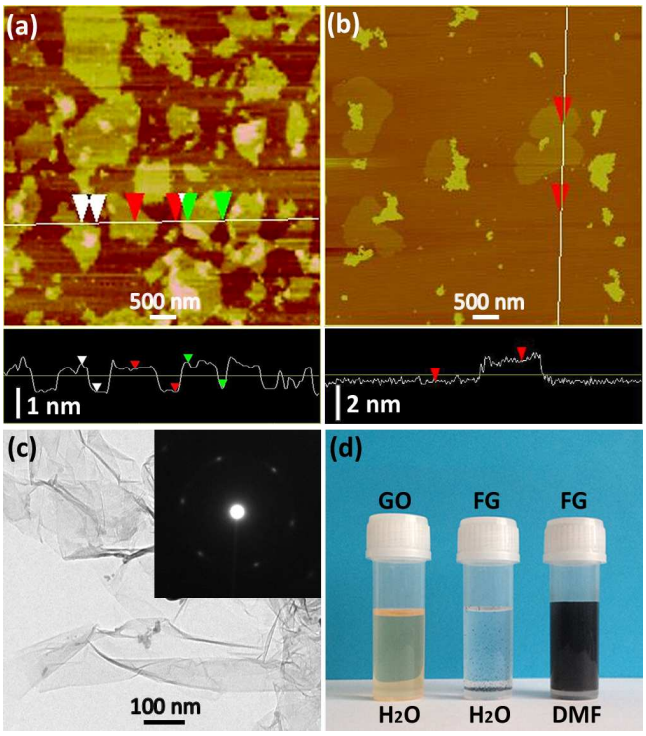

Figure 2. AFM images of (a) individually exfoliated GO and (b) FG sheets on freshly cleaved mica substrates and their corresponding height profiles along the given lines; (c) a typical TEM image of FG and SAED pattern of FG (inset); (d) optical pictures of GO dispersed in H_2O, FG in H_2O and DMF, respectively.

Figure 3a shows XPS scans of graphite, GO and FG powders. Pristine graphite consists of rich C and a small trace of O, while the peak intensity of O 1s (531 eV) is significantly increased with respect to the C 1s peak (285 eV) after oxidation to GO. The atomic ratio of C/O within GO is calculated to be ~2.1 by integrating peak area of C1s to O1s. After functionalization and reduction of GO to FG, its C/O ratio is raised to 5.27 but lower than the reported values (~7.5) for directly reduced GO.[37] This is attributable to the residual oxygen moieties of carbamate and amide bonds. Note that a new peak for FG appears at 400 eV due to N 1s which mainly originates from the NCO species of *m*-TMI. In the high-resolution core-level spectra (Fig. 3b), the "absent" signal of N 1s in GO is clearly observed in FG. The N content of FG is calculated to be ~1.7% while the intrinsic N content for *m*-TMI is ~7% based on its chemical formula. Thus it can be reevaluated to be ~24.3% of *m*-TMI present in FG by assuming that all N moieties are from *m*-TMI. However, chemical

reduction of GO with hydrazine derivate often results in partial N-doping of graphene,[38] and this implies that the real amount of N present in FG is slightly lower than ~24.3%.

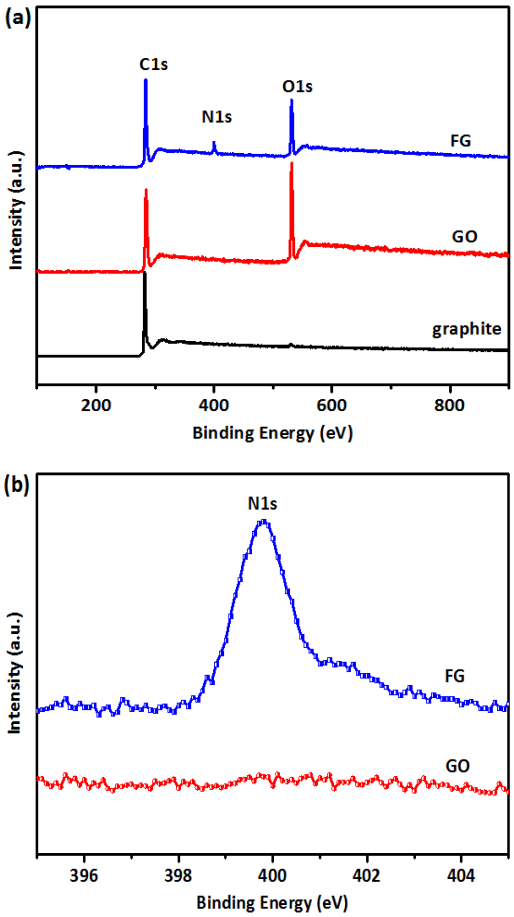

Figure 3. (a) XPS scans of graphite, GO and FG, and (b) high-resolution core-level spectra of N 1s of GO and FG sheets.

Figure 4 shows the Raman spectra of GO and FG. Two characteristic G and D bands usually correspond to the first-order scattering of the E_{2g} phonon and the breathing modes of κ-point photon of A_{1g} symmetry, respectively.[39, 40] Two fundamental vibrations clearly occur at 1590 and 1352 cm^{-1} for GO. However, the G band appears at 1583 cm^{-1} for PG with a red-shift of 7 cm^{-1} while retaining a minor blue-shift (1 cm^{-1}) for D band compared to GO. The location of G peak is close to that of pristine graphite (~1580 cm^{-1}), indicating the restoration of graphitic sp^2 network in FG during

chemical and solvothermal reduction.[41] Moreover, the intensity ratios (I_D/I_G) of D to G band were calculated by integrating their peak areas. I_D/I_G of GO is about 1.25 which increases to 1.42 for FG. This change suggests a decrease in the average size of sp^2 aromatic domains from graphene by creating numerous new graphitic domains upon reduction of GO. Similar phenomena have been frequently reported for GO and reduced GO.[37, 40, 42, 43] Combining the microscopic techniques and spectra analysis successfully proves the functionalization and reduction of GO.

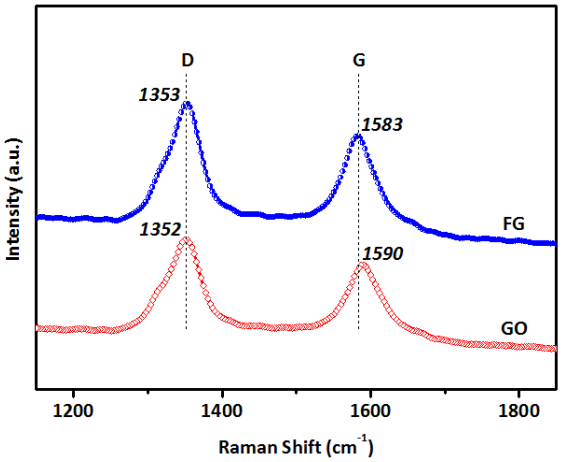

Figure 4. Raman spectra of GO and FG at an excitation wavelength of 514.5 nm.

Figure 5 shows the XRD pattern of graphite, GO, FG, PMMA and its composites with FG. A characteristic sharp (002) peak of graphite appears at 2θ=26.5°, which corresponds to an interlayer spacing of 0.34 nm.[44] After oxidization of graphite to GO, this (002) peak shifts downward to a lower angle (2θ=9.7°) with a corresponding spacing of 0.91 nm. This distance is close to the height (0.86 nm) of a single-layer GO sheet measured by AFM, but much larger than that of graphite since the intercalated oxygen-containing groups are contained within GO. However, no dominant peaks normally observed in graphite and GO can be detected for FG, which are intrinsically different from the graphite intercalation compounds.[45] This result indicates that FG may be exfoliated into individual sheets to form a highly disordered topology during covalent functionalization with

m-TMI. For graphene/PMMA composites, regardless of loading levels of FG, their XRD patterns have similar profiles revealing the amorphous peaks of neat PMMA. This implies that FG sheets do not re-aggregate in the matrix during *in-situ* polymerization and subsequent processing.[46]

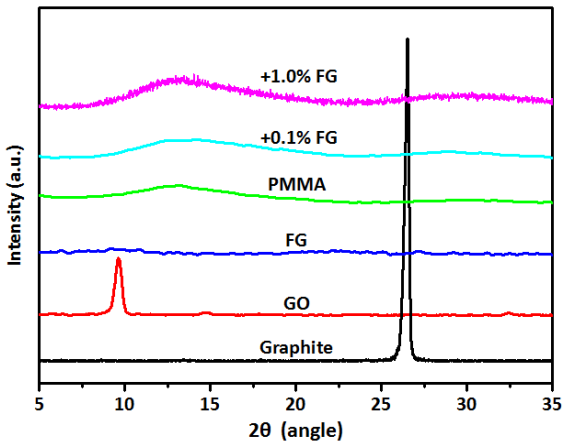

Figure 5. XRD patterns of graphite, GO, FG, neat PMMA and typical graphene/PMMA composites containing 0.1 and 1.0% of FG sheets.

The dispersion state of graphene sheets in the matrix was further studied by TEM and SEM techniques. As shown in Figure 6, most of crumpled graphene sheets are individually exfoliated and dispersed into the PMMA matrix over the loading levels studied. A few stacked-sheets can be observed for PMMA composites at relatively high loadings of FG (Fig. 6b, c), however, their lateral dimensions remain in the range of several hundred nanometres to micrometres. This wrinkled topology is due to the distortions of graphene caused by the residual oxygenated-groups, structural defects and extremely large aspect ratio. It clearly differs from the typically flat configuration of GO and FG sheets examined by AFM (Fig. 2) as they are deposited onto an atomically flat mica substrate, but not in a polymer matrix.[15] It is noted that a SEM charge contrast image for the fractured surface of 1% FG/PMMA composite seems to be fully covered by the wrinkled sheets (Fig. 6d) because of relatively good dispersion and large surface area of FG. This visual contrast

arises from the fact that the secondary electron yield is predominately enriched at the location of the electrically conductive FG sheets due to low charge-transport capacity of the insulating PMMA matrix.[47] Such homogeneity of graphene sheets is expected to show great improvements in the nanomechanical and thermal properties of PMMA composites.

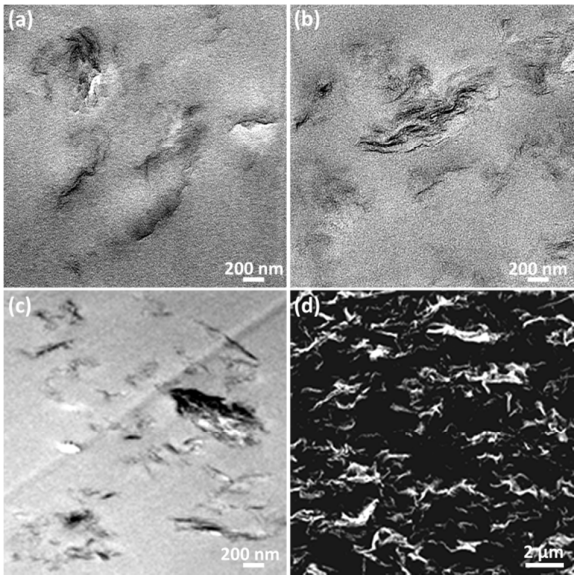

Figure 6. TEM images of PMMA composites with FG loading: (a) 0.3%, (b) 0.7%, and (c) 1.0%; (d) SEM charge contrast image of freshly fractured cross-sectional surface of 1% FG/PMMA composite.

3.2. Nanomechanical properties of graphene/PMMA composites

Molecular dynamics simulations based on nanoindentation models have identified a high Young's modulus of 1.0 TPa for monolayer graphene,[48] which promises to improve the nanomechanical properites of polymers. Figure 7 shows typical loading-holding-unloading curves of PMMA and its composites. The whole curves have no discontinuities or steps and steadily shift upward with increasing content of FG in PMMA, indicating that no cracks were formed during indentation.[49] The indentation forces at the peak load (P_m) gradually increase from 14.1 mN for neat PMMA to 21.1 mN by incorporating 1.0% FG into the matrix. This implies that the composites' resistance to indentation increases with FG filling.[22] Significant creep occurs clearly at the holding period of P_m

for PMMA and the composites, and this behavior is most readily observed for polymer-based materials during indentation tests.[19, 50, 51] However, the creep displacements at P_m only show a slight difference between the composites, suggesting that FG has little effect on the creep resistance of PMMA.[22]

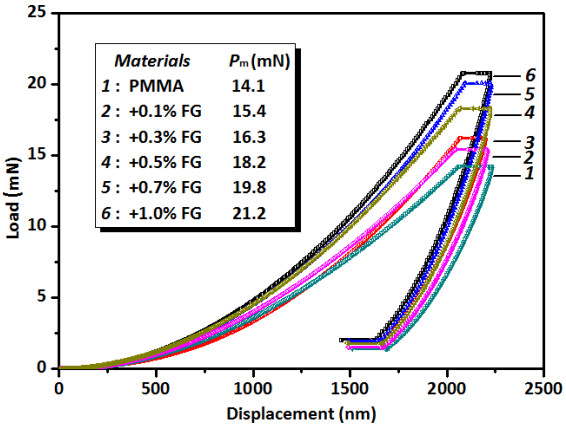

Figure 7. Representative load-displacement curves of indentations made at a maximum penetration depth of 2000 nm on neat PMMA and graphene/PMMA composites.

Figure 8 shows the elastic modulus (E) profiles with respect to the indentation depth and FG content for PMMA and its composites, respectively. The dramatic drops in E values before 250 nm are probably due to the indentation size effect.[22] However, these curves smoothly attain a plateau for the depths over 250 nm until 2000 nm (Fig. 8a), suggesting that graphene sheets are well dispersed in PMMA along the indentation direction.[22] E values of each specimen were thus obtained by averaging values of ten indentations in the plateau range of 500-2000 nm. As expected, E values of graphene/PMMA composites are higher than those of neat PMMA over the depth range tested (Fig. 8a), and gradually increase with graphene loading (Fig. 8b). Of note, E values of glassy polymers are principally governed by inter-chain interaction which is usually predominated by the relatively weak van der Waals force, and typically ranges from 2.5 to 4.5 GPa.[19] E for neat PMMA was here measured to be 3.25 GPa, comparable to previous values reported.[50, 52, 53] However, E'

values are 3.77 GPa for 0.1% FG and 5.62 GPa for 1.0% FG, yielding 16% and 72.9% increments, respectively. This significant reinforcement suggests that graphene sheets with intrinsic high strength are well dispersed in the matrix to show high contact area and strong interfacial adhesion with PMMA bridged by *m*-TMI. Similar improvements in *E* determined by nanoindentation have been reported for PMMA composites filled with few-layer graphene,[20] carbon nanotubes (CNTs),[54] Si_3N_4,[50] ZnO[55] and $Bi_{12}SiO_{20}$.[52] It should be pointed out that *E* of a polymer-based material obtained by the Oliver-Pharr method is significantly higher than the macroscopic Young's modulus due to the theoretic and experimental limitations as described elsewhere.[19]

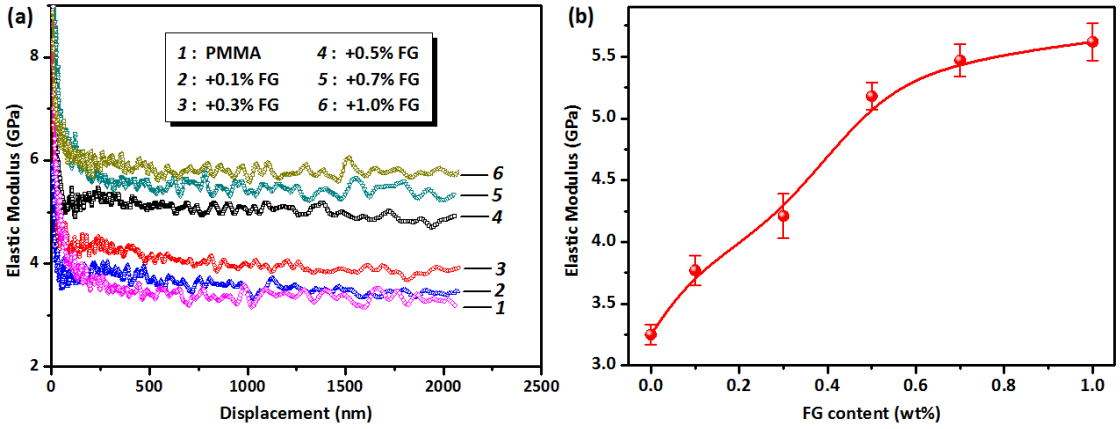

Figure 8. Elastic modulus plotted as a function of displacement (a) and FG content (b) for PMMA and its composites.

Figure 9 plots the indentation hardness (*H*) for PMMA and its composites as a function of contact depth and FG content, respectively. Like *E versus* displacement curves, the *H*-displacement profiles of all samples also exhibit stable trends after indentation depth approaches 250 nm and onward (Fig. 9a). *H* values are independent of the indentation displacement over 250 nm, but gradually increase for the composites with increasing FG loading (Fig. 9b). For instance, *H* is 164.5 MPa for neat PMMA and 248.8 MPa for PMMA with 1.0% FG, giving an increase by 51.2%. At a comparable loading (1 wt%), this increment (51.2%) is lower than that of CNT/nylon 6 composites

(84%),[22] but higher than those of SiO_2/epoxy (9.0%),[56] CNT/epoxy (13%)[23] and $Bi_{12}SiO_{20}$/PMMA (34.2%)[52] composites. Considering that graphene has comparable mechanical strength to CNTs, the greater improvement in *H* for nylon 6 should originate from the dominant formation of thermodynamically stable α-phase crystals induced by acid-treated CNTs in the composites.[22] However, *H* of a material is defined as the resistance to the deformation caused by normal force,[57] and hence depends on the effective filler-matrix load transfer.[20] The low intrinsic strength of both SiO_2 and $Bi_{12}SiO_{20}$ and weak interface adhesion with the matrix thus provide with low mechanical reinforcement for their epoxy and PMMA composites.[52,56] Direct incorporation of unmodified CNTs into an epoxy resin often results in a weak interface and poor dispersion and hence, relatively low enhancement in *H*.[23] In this work, graphene sheets have high strength and are also chemically coupled with PMMA which results in a reinforcement for the matrix against the deformation and a strong interface for load transfer. In addition, the average standard deviations of *E* and *H* values (ten tests) for the composites vary from 0.12 GPa to 0.18 GPa, and from 7.6 MPa to 15.2 MPa, respectively, as shown in the error bars in the graphs (Fig. 8b, Fig. 9b). These standard deviations are relatively small, further implying a good dispersion of graphene sheets throughout the matrix.

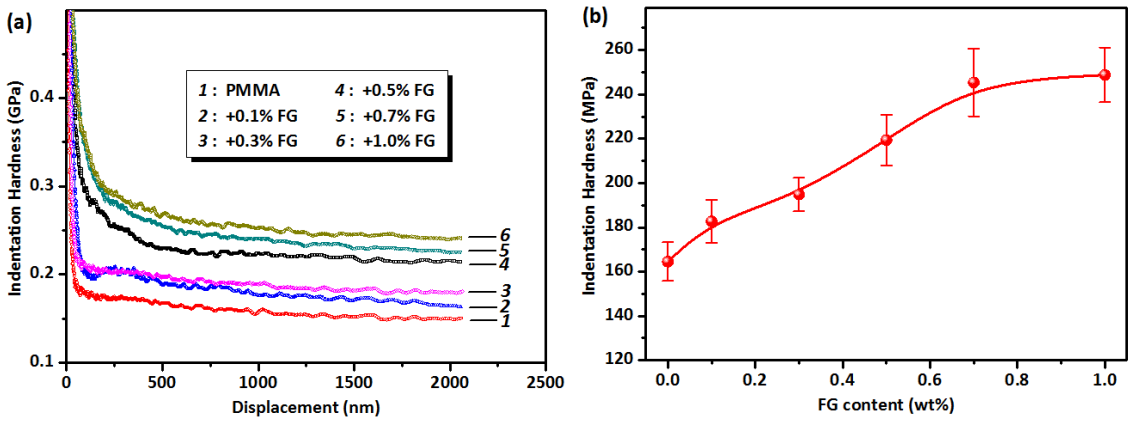

Figure 9. Indentation hardness (*H*) plotted as a function of displacement (a) and FG content (b) for PMMA and its composites.

Recent studies have attempted to evaluate the elastic-plastic response of polymeric materials by means of the load-displacement diagrams of nanoindentation test.[23, 52, 56-58] Two parameters of plasticity index (ψ) and recovery resistance (R_s) are proposed for the purpose. For polymeric materials, ψ ranges from 0 to 1, wherein the upper and lower limits represent fully-plastic and fully-elastic behavior of materials, respectively. R_s is an indicator of the energy dissipation during nanoindentation test. Figure 10 shows ψ and R_s values of PMMA and its composites as a function of FG content. The ψ value of neat PMMA is 0.588 comparable to the literature value,[21] but gradually decreases to 0.516 with increasing FG content to 1.0% (Fig. 10a). By contrast, the R_s value of neat PMMA was calculated to be 183 GPa and gradually increases to 361.8 GPa at 1.0% FG loading (Fig. 10b). A decrease in ψ and an increase in R_s suggest that incorporation of graphene into PMMA changes the elastic-plastic behavior by increasing the portion related to the elastic work.[23] The higher FG loading results in a larger reduction of ψ and hence, a greater improvement in the elastic recovery of the composites and less plastic deformation remaining. Moreover, the improved elastic recovery of the material surface is clearly reflected by gradual decrease of final depth (see Fig. 7) after test in the presence of more nano-reinforcements. Similar change trends of ψ and R_s have been observed for graphene/vinyl ester resin,[57] CNT/epoxy,[23] SiO_2/PC,[59] and SiO_2/epoxy[56] composites.

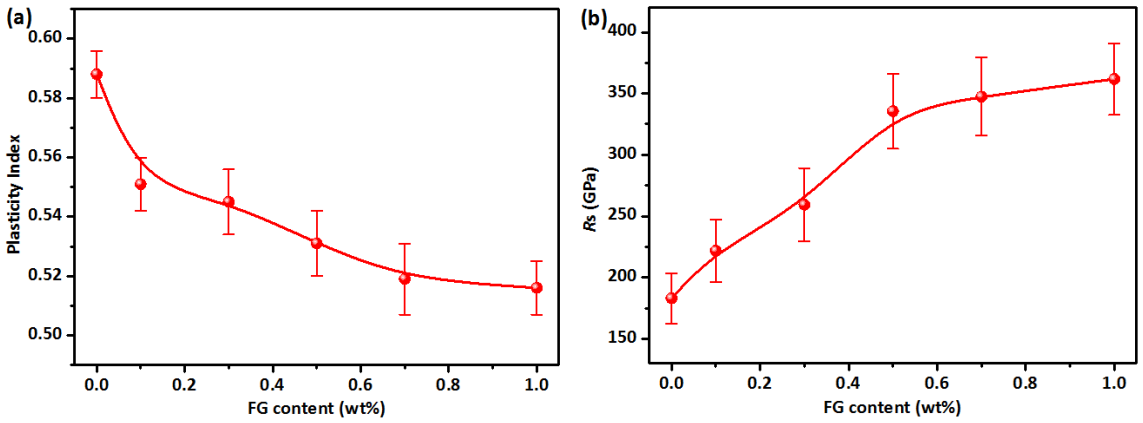

Figure 10. (a) Plasticity index (ψ) and (b) recovery resistance (R_s) parameters plotted as a function of FG content for PMMA and its composites.

3.3. Thermal properties of graphene/PMMA composites

Figure 11 DSC curves of neat PMMA and graphene/PMMA composites. Glass transition temperatures (T_gs) of composites gradually shift to higher temperatures with increasing graphene loading. T_g is 95.4°C for neat PMMA and 108.1°C for PMMA with 1% graphene, giving an increase by 12.7°C. The improvement in T_g for graphene/PMMA composites can be explained by two factors. First, the wrinkled and crumpled graphene sheets (see Fig. 6) represent nanoscale surface roughness that promotes mechanical interlocking with PMMA chains.[60] Both molecular dynamics simulation[61] and experimental data[62] have shown that the mobility of polymer chains is geometrically restricted in the vicinity of a nanoparticle surface or interface. Second, *m*-TMI bridges between PMMA chains and graphene through covalent bonding. These synergic effects produce significant geometric constraints on the mobility of PMMA chains, thereby enhancing T_g.

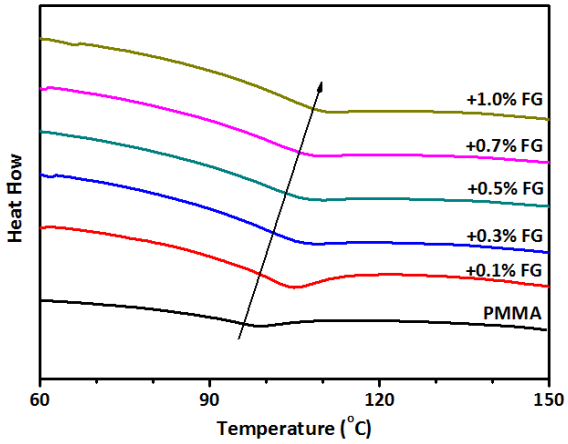

Figure 11. DSC thermograms of neat PMMA and graphene/PMMA composites.

The thermal stability of neat PMMA and graphene/PMMA composites was examined by TGA under inert atmosphere. As shown in Figure 12, the thermal decomposition temperatures gradually increase with graphene loading. For example, the onset decomposition temperature (at 5% weight loss) increases from ~180°C of neat PMMA to ~280°C by addition of 1% FG. The enhanced

resistance to degradation arises intrinsically from high thermal stability of graphene. Meanwhile, graphene sheets, by analogy with clay layers,[63, 64] may behave as an efficient barrier for reducing permeability of volatile gas during thermal decomposition. The heat transport is thus retarded by slowing out-diffusion and migration of volatile molecules from the inner matrix to the surface, enabling higher decomposition temperatures. In addition, neat PMMA and its composites with low filling undergo three steps of weight loss caused by the scissions of head-to-head linkages, unsaturated vinylidene ends and polymer chains with increasing temperature. This is a general phenomenon for radically polymerized PMMA as reported.[65] In contrast, thermal degradation of PMMA composites with high loading shows two distinguishable steps possibly owing to the gas barrier property of graphene sheets which makes it difficult to differentiate the three decomposition stages of PMMA. Similar observations can also be found in other graphene/PMMA composites.[66]

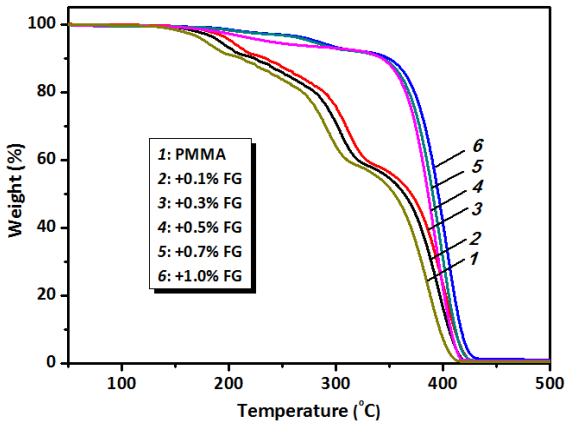

Figure 12. TGA thermograms of neat PMMA and graphene/PMMA composites.

4. Conclusions

GO reacted with *m*-TMI and then underwent chemical reduction with dimethylhydrazine and solvothermal reduction in DMF. The resulting functionalized-graphene is hydrophobic and stable in polar solvents. Covalent coupling of graphene into the PMMA matrix was achieved by *in-situ* polymerization of MMA in the presence of graphene-containing reactive vinyl-benzyl groups.

Well-dispersed graphene sheets form strong interface bonding with the PMMA matrix and hence, contributing to large increases in elastic modulus (+72.9%) and indentation hardness (+51.2%) for the PMMA composites filled with 1 wt% of graphene. The onset decomposition temperature and glass transition temperature of neat PMMA also increased by 100°C and 12.7°C, respectively. Besides, incorporation of FG into PMMA changed its elastic-plastic behavior, resulting in a decrease of plasticity index and an increase of recovery resistance for the resulted composites. For this work, a general method has been developed and could be extended to other vinyl polymer-based composites containing graphene.

Acknowledgements

We acknowledge the financial support from the National Natural Science Foundation of China (51073050, 51273057 and 51210004), the Program for New Century Excellent Talents in University (NCET-12-0709) and the Open Project of State Key Laboratory of Materials Processing and Die & Mould Technology (2012-P10) at Huazhong University of Science and Technology. CPT would like to thank for the support from Research Committee of The Hong Kong Polytechnic University (G-UB32).

References

1. M. J. Allen, V. C. Tung and R. B. Kaner, *Chem. Rev.*, 2010, **110**, 132-145.
2. T. Kuilla, S. Bhadra, D. Yao, N. H. Kim, S. Bose and J. H. Lee, *Prog. Polym. Sci.*, 2010, **35**, 1350-1375.
3. S. Park and R. S. Ruoff, *Nat. Nanotechnol.*, 2009, **4**, 217-224.
4. R. Verdejo, M. M. Bernal, L. J. Romasanta and M. A. Lopez-Manchado, *J. Mater. Chem.*, 2011, **21**, 3301-3310.
5. H. Kim, A. A. Abdala and C. W. Macosko, *Macromolecules*, 2010, **43**, 6515-6530.
6. R. G. Peng, Y. Z. Wang, W. Tang, Y. K. Yang and X. L. Xie, *Polymers*, 2013, **5**, 847-872.
7. J. R. Potts, D. R. Dreyer, C. W. Bielawski and R. S. Ruoff, *Polymer*, 2011, **52**, 5-25.

8. H. Bai, C. Li and G. Shi, *Adv. Mater.*, 2011, **23**, 1089-1115.
9. G. Goncalves, P. A. A. P. Marques, A. Barros-Timmons, I. Bdkin, M. K. Singh, N. Emami and J. Gracio, *J. Mater. Chem.*, 2010, **20**, 9927-9934.
10. M. Fang, K. Wang, H. Lu, Y. Yang and S. Nutt, *J. Mater. Chem.*, 2010, **20**, 1982-1992.
11. Y. Tan, L. Fang, J. Xiao, Y. Song and Q. Zheng, *Polym. Chem.*, 2013, **4**, 2939-2944.
12. S. Jiang, Z. Gui, C. Bao, K. Dai, X. Wang, K. Zhou, Y. Shi, S. Lo and Y. Hu, *Chem. Eng. J.*, 2013, **226**, 326-335.
13. W. Y. Xu and J. Smid, *Macromolecules*, 1993, **26**, 7004-7008.
14. L. Barner, C. Barner-Kowollik and T. P. Davis, *J. Polym. Sci. Pol. Chem.*, 2002, **40**, 1064-1074.
15. S. Stankovich, D. A. Dikin, G. H. B. Dommett, K. M. Kohlhaas, E. J. Zimney, E. A. Stach, R. D. Piner, S. T. Nguyen and R. S. Ruoff, *Nature*, 2006, **442**, 282-286.
16. C. Xu, X. Wu, J. Zhu and X. Wang, *Carbon*, 2008, **46**, 386-389.
17. N. I. Kovtyukhova, P. J. Ollivier, B. R. Martin, T. E. Mallouk, S. A. Chizhik, E. V. Buzaneva and A. D. Gorchinskiy, *Chem. Mater.*, 1999, **11**, 771-778.
18. Y. Yang, C.-E. He, R.-G. Peng, A. Baji, X. Du, Y.-L. Huang, X. Xie and Y.-W. Mai, *J. Mater. Chem.*, 2012, **22**, 5666-5675.
19. J. M. Kranenburg, C. A. Tweedie, K. J. van Vliet and U. S. Schubert, *Adv. Mater.*, 2009, **21**, 3551-3561.
20. B. Das, K. E. Prasad, U. Ramamurty and C. N. R. Rao, *Nanotechnology*, 2009, **20**, 125705.
21. B. J. Briscoe, L. Fiori and E. Pelillo, *J. Phys. D: Appl. Phys.*, 1998, **31**, 2395.
22. T. X. Liu, I. Y. Phang, L. Shen, S. Y. Chow and W. D. Zhang, *Macromolecules*, 2004, **37**, 7214-7222.
23. M. R. Ayatollahi, S. Doagou-Rad and S. Shadlou, *Macromol. Mater. Eng.*, 2012, **297**, 689-701.
24. W. C. Oliver and G. M. Pharr, *J. Mater. Res.*, 1992, 7, 1564-1583.
25. J. I. Paredes, S. Villar-Rodil, A. Martínez-Alonso and J. M. D. Tascón, *Langmuir*, 2008, **24**, 10560-10564.
26. A. Lerf, H. He, M. Forster and J. Klinowski, *J. Phys. Chem. B*, 1998, **102**, 4477-4482.
27. W. Cai, R. D. Piner, F. J. Stadermann, S. Park, M. A. Shaibat, Y. Ishii, D. Yang, A. Velamakanni, S. J. An, M. Stoller, J. An, D. Chen and R. S. Ruoff, *Science*, 2008, **321**, 1815-1817.
28. S. Stankovich, D. Dikin, R. Piner, K. Kohlhaas, A. Kleinhammes, Y. Jia, Y. Wu, S. Nguyen and R. Ruoff, *Carbon*, 2007, **45**, 1558-1565.
29. X. Wang, Y. Hu, L. Song, H. Yang, W. Xing and H. Lu, *J. Mater. Chem.*, 2011, **21**, 4222-4227.
30. J. R. Lomeda, C. D. Doyle, D. V. Kosynkin, W. F. Hwang and J. M. Tour, *J. Am. Chem. Soc.*, 2008, **130**, 16201-16206.
31. M. Fang, K. G. Wang, H. B. Lu, Y. L. Yang and S. Nutt, *J. Mater. Chem.*, 2009, **19**, 7098-7105.
32. O. Baoli, Z. Zhihua, L. Qingquan, L. Bo, Y. Shoujun, O. Yangjian, Z. Xin and L. Duxin, *Polym. Chem.*, 2012, **3**, 2768-2775.
33. O. C. Compton, B. Jain, D. A. Dikin, A. Abouimrane, K. Amine and S. T. Nguyen, *Acs Nano*, 2011, **5**, 4380-4391.
34. H. Wang, J. T. Robinson, X. Li and H. Dai, *J. Am. Chem. Soc.*, 2009, **131**, 9910-9911.

35. Y. J. Guo, S. J. Guo, J. T. Ren, Y. M. Zhai, S. J. Dong and E. K. Wang, *Acs Nano*, 2010, **4**, 4001-4010.
36. J. M. Englert, C. Dotzer, G. A. Yang, M. Schmid, C. Papp, J. M. Gottfried, H. P. Steinruck, E. Spiecker, F. Hauke and A. Hirsch, *Nat. Chem.*, 2011, **3**, 279-286.
37. H.-J. Shin, K. K. Kim, A. Benayad, S.-M. Yoon, H. K. Park, I.-S. Jung, M. H. Jin, H.-K. Jeong, J. M. Kim, J.-Y. Choi and Y. H. Lee, *Adv. Funct. Mater.*, 2009, **19**, 1987-1992.
38. C. K. Chua and M. Pumera, *Chem. Soc. Rev.*, 2014, **43**, 291-312.
39. Z. J. Fan, W. Kai, J. Yan, T. Wei, L. J. Zhi, J. Feng, Y. M. Ren, L. P. Song and F. Wei, *Acs Nano*, 2011, **5**, 191-198.
40. Y. Guo, S. Guo, J. Ren, Y. Zhai, S. Dong and E. Wang, *Acs Nano*, 2010, **4**, 4001-4010.
41. H. B. Zhang, J. W. Wang, Q. Yan, W. G. Zheng, C. Chen and Z. Z. Yu, *J. Mater. Chem.*, 2011, **21**, 5392-5397.
42. Y. Zhou, Q. L. Bao, L. A. L. Tang, Y. L. Zhong and K. P. Loh, *Chem. Mater.*, 2009, **21**, 2950-2956.
43. W. Gao, L. B. Alemany, L. J. Ci and P. M. Ajayan, *Nat. Chem.*, 2009, **1**, 403-408.
44. H.-K. Jeong, Y. P. Lee, R. J. W. E. Lahaye, M.-H. Park, K. H. An, I. J. Kim, C.-W. Yang, C. Y. Park, R. S. Ruoff and Y. H. Lee, *J. Am. Chem. Soc.*, 2008, **130**, 1362-1366.
45. B. Ozmen-Monkul and M. M. Lerner, *Carbon*, 2010, **48**, 3205-3210.
46. J. Liang, Y. Huang, L. Zhang, Y. Wang, Y. Ma, T. Guo and Y. Chen, *Adv. Funct. Mater.*, 2009, **19**, 2297-2302.
47. V. H. Pham, T. T. Dang, S. H. Hur, E. J. Kim and J. S. Chung, *Acs Appl. Mater. Interfaces*, 2012, **4**, 2630-2636.
48. T. Xinjun, W. Jian, Z. Kaiwang, P. Xiangyang, S. Lizhong and Z. Jianxin, *Appl. Phys. Lett.*, 2013, **102**, 071908.
49. X. F. Li, K. T. Lau and Y. S. Yin, *Compos. Sci. Technol.*, 2008, **68**, 2876-2881.
50. C. Shi, Y. Zhu, H. Qian and L. Lu, *Mater. Res. Bull.*, 2014, **51**, 161-166.
51. M. Ghorbanzadeh Ahangari, A. Fereidoon, M. Jahanshahi and N. Sharifi, *Compos. B: Eng.*, 2014, **56**, 450-455.
52. R. M. Dukali, I. Radovic, D. B. Stojanovic, P. S. Uskokovic, N. Romcevic, V. Radojevic and R. Aleksic, *J. Alloys Comp.*, 2014, **583**, 376-381.
53. L. Brown, T. Koerner, J. H. Horton and R. D. Oleschuk, *Lab on a Chip*, 2006, **6**, 66-73.
54. M. Olek, K. Kempa, S. Jurga and M. Giersig, *Langmuir*, 2005, **21**, 3146-3152.
55. H. Chakraborty, A. Sinha, N. Mukherjee, D. Ray and P. Protim Chattopadhyay, *Mater. Lett.*, 2013, **93**, 137-140.
56. Z.-Z. Wang, P. Gu, X.-P. Wu, H. Zhang, Z. Zhang and M. Y. M. Chiang, *Compos. Sci. Technol.*, 2013, **79**, 49-57.
57. M. M. Shokrieh, M. R. Hosseinkhani, M. R. Naimi-Jamal and H. Tourani, *Polym. Test.*, 2013, **32**, 45-51.
58. Y. Zamani Ketek Lahijania, M. Mohseni and S. Bastani, *Tribol. Inter.*, 2014, **69**, 10-18.
59. H. Zhang, H. Zhang, L. Tang, L. Zhou, C. Eger and Z. Zhang, *Compos. Sci. Technol.*, 2011, **71**, 471-479.
60. T. Ramanathan, A. A. Abdala, S. Stankovich, D. A. Dikin, M. Herrera-Alonso, R. D. Piner, D. H. Adamson, H. C. Schniepp, X. Chen, R. S. Ruoff, S. T. Nguyen, I. A. Aksay, R. K. Prud'homme and L. C. Brinson, *Nat.*

Nanotechnol., 2008, **3**, 327-331.

61. F. W. Starr, T. B. Schrøder and S. C. Glotzer, *Macromolecules*, 2002, **35**, 4481-4492.
62. P. Rittigstein, R. D. Priestley, L. J. Broadbelt and J. M. Torkelson, *Nat. Mater.*, 2007, **6**, 278-282.
63. M. Zanetti, G. Camino, P. Reichert and R. Mülhaupt, *Macromol. Rapid Comm.*, 2001, **22**, 176-180.
64. L. Cui, N. H. Tarte and S. I. Woo, *Macromolecules*, 2008, **41**, 4268-4274.
65. T. Kashiwagi, A. Inaba, J. E. Brown, K. Hatada, T. Kitayama and E. Masuda, *Macromolecules*, 1986, **19**, 2160-2168.
66. J. R. Potts, S. H. Lee, T. M. Alam, J. An, M. D. Stoller, R. D. Piner and R. S. Ruoff, *Carbon*, 2011, **49**, 2615-2623.